

Comparative Study of Foreign Object and Misalignment in Inductive Power Transfer Systems

Shi, Wenli; Dong, Jianning; Bandyopadhyay, Soumya; Grazian, Francesca; Soeiro, Thiago Batista; Bauer, Pavol

DOI

[10.1109/IECON.2019.8926782](https://doi.org/10.1109/IECON.2019.8926782)

Publication date

2019

Document Version

Final published version

Published in

IECON 2019 - 45th Annual Conference of the IEEE Industrial Electronics Society

Citation (APA)

Shi, W., Dong, J., Bandyopadhyay, S., Grazian, F., Soeiro, T. B., & Bauer, P. (2019). Comparative Study of Foreign Object and Misalignment in Inductive Power Transfer Systems. In *IECON 2019 - 45th Annual Conference of the IEEE Industrial Electronics Society* (pp. 2634-2639). Article 8926782 IEEE. <https://doi.org/10.1109/IECON.2019.8926782>

Important note

To cite this publication, please use the final published version (if applicable). Please check the document version above.

Copyright

Other than for strictly personal use, it is not permitted to download, forward or distribute the text or part of it, without the consent of the author(s) and/or copyright holder(s), unless the work is under an open content license such as Creative Commons.

Takedown policy

Please contact us and provide details if you believe this document breaches copyrights. We will remove access to the work immediately and investigate your claim.

Green Open Access added to TU Delft Institutional Repository

'You share, we take care!' - Taverne project

<https://www.openaccess.nl/en/you-share-we-take-care>

Otherwise as indicated in the copyright section: the publisher is the copyright holder of this work and the author uses the Dutch legislation to make this work public.

Comparative Study of Foreign Object and Misalignment in Inductive Power Transfer Systems

Wenli Shi, Jianning Dong, Soumya Bandyopadhyay, Francesca Grazian, Thiago Batista Soeiro, Pavol Bauer
Dept. Electrical Sustainable Energy, DCE&S group
TU Delft, Mekelweg 04, 2628 CD, Delft, the Netherlands
E-mail: W.Shi-3, J.Dong-4, P.Bauer@tudelft.nl

Abstract—This paper aims to identify the difference between foreign object (FO) and misalignment in terms of their influence on inductive power transfer (IPT) systems. This is performed through magnetic and equivalent circuit analysis of the mutual inductance, primary input impedance, charging pad terminal impedance and current harmonics. Experiment measurements on an IPT prototype are carried out to verify the analysis. It is found that: the charging pad terminal impedance under FO condition has a more pronounced decrement than that of misalignment; the mutual inductance under FO condition shows negative correlation with frequency, while positive for misalignment; the absolute value of the input impedance is decreased by FO and increased by misalignment; the influence of FO and misalignment on the THD of the input current is minimal. Finally, it is possible to detect FO and distinguish it from misalignment, through the variation of the primary pad terminal inductance, as well as the frequency dependence of the primary input impedance and the mutual inductance.

Keywords—inductive power transfer, foreign objects, misalignment, current harmonics, wireless power transfer.

I. INTRODUCTION

The inductive power transfer technique has gained extensive attention as it enables energy transfer over a large air gap. Since there is no mechanical contact between the primary and secondary charging pads, IPT system can be sealed, which makes it resistive to dust, water, and chemicals [1]. With a tradeoff between the power transfer distance and efficiency, IPT technique is increasingly popularized in both the low-power devices like biomedical implants, smartphones and the high-power equipment including factory automation, and the charging of electric vehicles (EVs).

A Dynamic IPT (DIPT) system makes it possible to charge EVs while driving on the road. This technique can be used as a strategy to reduce the battery size and/or extend the driving range of the vehicle. Typically, the transmitters are buried along the road, in the form of segmented pads or elongated tracks. FO is likely to be present on roads. If a FO is conductive, like canned drinks and coins, eddy current will be induced across the object when the transmitters are energizing. The eddy current produces heat causing a fire hazard, and generates magnetic field counteracting the source field. Therefore, system parameters like the coil leakage and mutual inductances may change due to the presence of FO. As a consequence, the system performances, including the current waveform and the power conversion efficiency will be affected. Thus, it is essential to detect FOs during the operation and remove them or temporarily shut down the nearby transmitters.

In the field of inductive EV charging, a few methods to detect FO are reported, which involves the detection of changes on the system parameters, such as the coil quality factor [2], resonant or cut-off frequency [3], power conversion efficiency [4] and induced voltage [5], [6]. Coil arrays dedicated to FO

detection are reported in [5], [6]. Overlapped detection coil is developed by WiTricity to sense the imbalanced voltage resulted from any metal-based object [6]. When metal objects are not present over the coil, the detection voltage is null. In order to remove the blind zone at every intersection point of the coils, an extra set of interleaved detection coils is added. Detection method applying non-overlapped coils is presented in [5]. Two coil arrays are configured longitudinally and laterally. This structure enables the detection device to determine the presence of metal objects by the induced voltage difference, as well as the position of the EV by the induced voltage. However, coil arrays increase the manufacturing and operation complexity.

It is also possible to detect FOs from the metric power conversion efficiency of the system since an extra loss is generated from the eddy current circulating across the FO. In [4], the power efficiency with and without addition of metal objects are compared. If this metric deviates from the normal value to a certain degree, an identification of a FO is reported. This method has been proved to be cost-effective and simple, but its application is commonly limited to low power IPT applications [7]. This mainly occurs because in high power applications the losses caused by the FOs are fairly low when compared to the rated active power, which makes the detection more complex. Other methods can be based on the detection of the IPT quality factor and/or the coupling coefficient of the coils as those are also affected by the presence of metal objects [2]. However, the misalignment between the transmitter and the receiver coils can also change the IPT quality factor. Therefore, the detection method cannot simply identify if the cause of parametric changes are due to a FO or just a case of coil misalignment.

In the DIPT system, the misalignment fluctuates in a large region. There is a high chance that the mutual coupling falls to zero in large misalignment, which poses challenges to reduce the power pulsation and maintain the efficiency at a considerate level. In terms of the influence of misalignment and FO, they both result in system parameters variation and system performance degradation. In order to identify appropriate FO detection methods, it is essential to compare how FOs and coil misalignment affect the operation of the DIPT system.

This paper investigates how coil misalignment and the presence of FOs affect the IPT system using circuit analysis. The mutual inductance and the primary input impedance are analyzed. In order to evaluate the characteristics of FOs, the parameters identification method is also introduced. Finally, measurements on a 3.3 kW IPT prototype are analyzed and possible FO detection methods are proposed.

II. INFLUENCE OF FOS AND COIL MISALIGNMENT

This section analyses the influence of the presence of FO and coil misalignment on the magnetic field and the IPT circuit parameters. The FO investigated is nonmagnetic and conductive,

and placed on top of the primary pad. Due to the limited size, the coupling between the secondary pad and the FO is neglected.

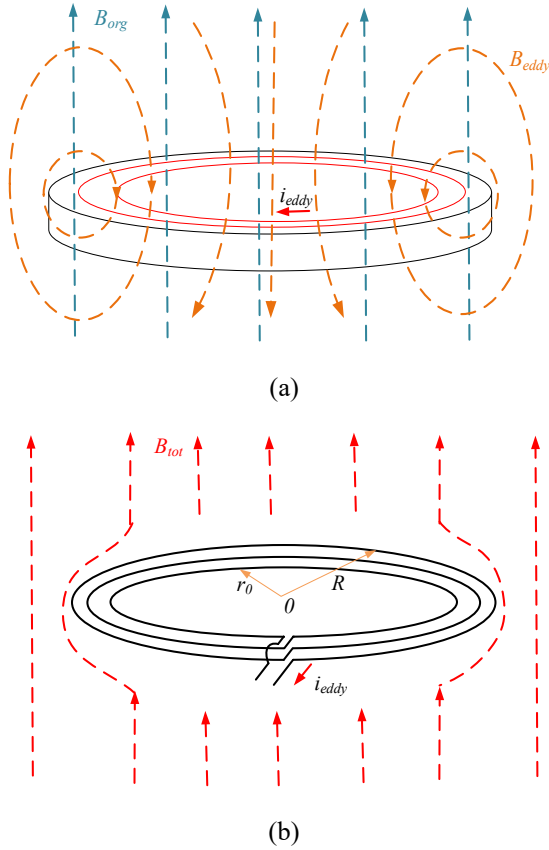


Fig. 1. (a) Metal object in uniform B field; (b) the equivalent circuit and magnetic field.

A. Mutual inductance

As shown in Fig. 1(a), a thin cylinder metal object is placed in a uniform alternating B field. According to Faraday's law, eddy current is induced within the object and generate a counteracting magnetic field. Due to the skin effect, the current is mainly distributed around the outer layer of the cylinder and perpendicular to the original field. On one hand, the eddy current will distract the magnetic field surrounded. On the other hand, energy is consumed because of the material resistivity and dissipated as heat. Thus, a FO can be considered as a practical coil, named FO coil, with a finite quality factor, as shown in Fig. 1(b).

Assume that the original field is produced by a source coil with a number of turns N_1 and current i_1 , and the FO has an equivalent total number of turns N_2 , distributed turns function $N_2(r)$ denoting the number of turns of the coil at radius r . The collection of r_i is $[r_0, r_1, \dots, r_n]$, where $r_n = R$. The flux through the coil at radius r can be expressed as

$$\varphi(r) = N_2(r) \frac{N_1 i_1}{R_m(r)} \quad (1)$$

where $R_m(r)$ is the reluctance of the flux through the area of the coil with radius r . The mutual inductance between the source and coupled coils is calculated with

$$M = \frac{\sum_{i=0}^n N_2(r_i) \frac{N_1 i_1}{R_m(r_i)}}{i_1} = \sum_{i=0}^n \frac{N_2(r_i) N_1}{R_m(r_i)} \quad (2)$$

Since the field frequency determines the distribution of eddy current in Fig 1(a), the distributed turns function changes with the field frequency. Besides, the location of the FO is random, so the magnetic reluctance differs at the different relative position between FO and the source coil. Thus, the mutual inductance of the FO coil at location p is expressed as

$$M_f = \sum_{i=0}^n \frac{N_{2-f}(r_i, \omega) N_1}{R_{m-f}(r_i, p)} \quad (3)$$

B. IPT impedance with the presence of a FO

Replacing the source coil with the primary charging pad and neglecting the parasitic capacitance of the coil, the equivalent circuit can be illustrated as shown in Fig. 2. C_1, C_2 are tuned at the switching frequency 85kHz. R_f and L_f denote the equivalent inductance and resistance of the FO, respectively.

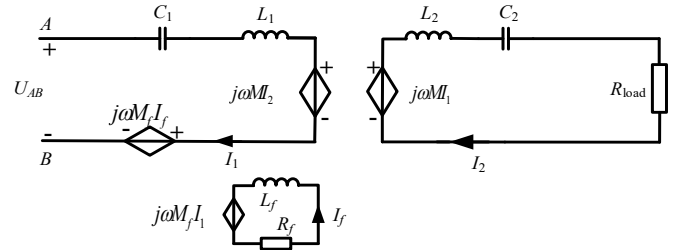


Fig. 2. Equivalent coupling circuit with the presence of FO.

The total reflected impedance of the secondary side and FO on the primary side is

$$Z_{ref-f} = \frac{\omega^2 M_f^2}{j\omega L_f + R_f} + \frac{\omega^2 M^2}{j\omega L_2 + \frac{1}{j\omega C_2} + R_{load}} \quad (4)$$

The input impedance of the primary side is

$$Z_{in-f} = \frac{\omega^2 M^2}{R_{load} + j\omega L_2 + \frac{1}{j\omega C_2}} + \frac{\omega^2 M_f^2}{j\omega L_f + R_f} + j\omega L_1 + \frac{1}{j\omega C_1} \quad (5)$$

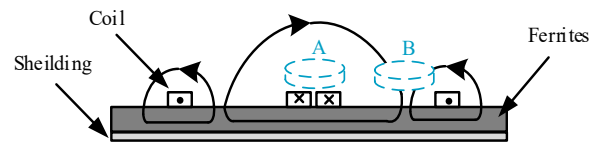


Fig. 3. 2D axial symmetric primary DD charging pad with FO.

As shown in Fig. 3, the investigated FO is placed at point A (centered point), the symmetric center of the charging pad, or point B (sided point), the symmetric center of one rectangular coil. At point A, the flux is 0 because of the symmetric magnetic field produced by the DD coil. From (2), we can see that there is no coupling in this case. At point B, the source magnetic field is almost perpendicular to the planar side of the object, so a strong

coupling exists between the metal object and the primary pad. From (5), it can be seen that the input impedance of the primary pad varies when M_f changes.

C. Impedance under misalignment

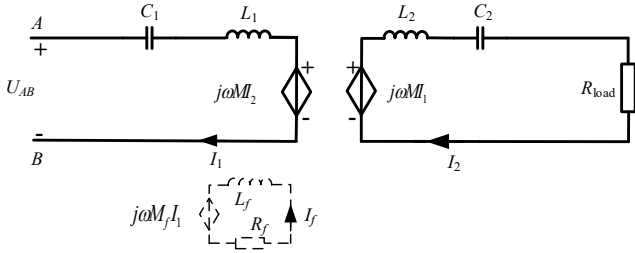


Fig. 4. Equivalent circuit of IPT without FO.

Because the primary and secondary side charging pads stay misaligned most of the time in a DIPT application, misalignment has to be considered in the system design. The variation of the relative position and angle between the charging pads changes the mutual inductance. According to (2), R_m changes at different coupling conditions. Different from a FO case, the secondary charging pad consists of a coil as well as ferrites and aluminum shielding, which can also modify the coupling between the charging pads. The mutual inductance between charging pads can be expressed as

$$M_{mis} = \alpha_{f,s} \sum_{i=0}^n \frac{N_{2_mis}(r_i)N_1}{R_{m_mis}(r_i)} \quad (6)$$

where $\alpha_{f,s}$ represents the effect of ferrite and shielding on the magnetic field. It is a function of frequency since the shielding effect is more dominant at high frequency.

The reflected impedance of the secondary pad is

$$Z_{ref_mis} = \frac{\omega^2 M_{mis}^2}{j\omega L_2 + \frac{1}{j\omega C_2} + R_{load}} \quad (7)$$

The input impedance of the primary pad is

$$Z_{in_mis} = \frac{\omega^2 M_{mis}^2}{R_{load} + j\omega L_2 + \frac{1}{j\omega C_2}} + j\omega L_1 + \frac{1}{j\omega C_1} \quad (8)$$

It can be seen from (5) and (8) that FO and misalignment affect the input impedance in a different way. A FO introduces extra coupling and works as an inductor and a resistor in series, while the misalignment weakens the coupling between the charging pads.

III. PARAMETERS IDENTIFICATION OF FOS

In Fig 1(b), a FO is simplified as a practical coil with finite quality factor. In practice, the inductance and resistance of a real coil can be easily measured through the terminals. However, for a solid FO which is equivalent to a virtual coil shown in Fig. 1(a), it is difficult to measure the terminal parameters. As shown in (5), the primary input impedance changes due to the coupling between the primary pad and the FO. Conversely, the primary

input impedance can reflect the influence of the FO. In order to simplify the analysis, only the primary charging pad and FO are considered, while the secondary charging pad and the parasitic parameters are neglected. The equivalent circuit is shown in Fig. 5. The primary pad terminal inductance L_{It} and resistance R_{It} are defined to satisfy $Z_{It} = j\omega L_{It} + R_{It}$, where Z_{It} is the terminal impedance.

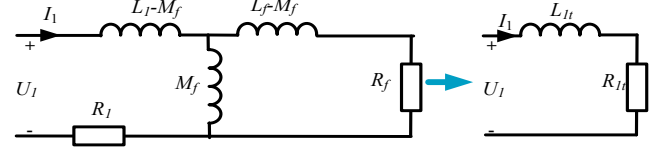


Fig. 5. Equivalent circuit of the primary pad coupled with FO.

By measuring the variation of the input impedance caused by a FO, it is possible to solve L_{It} and R_{It} . According to Fig. 5, one can get

$$\begin{cases} R_{It} = \frac{L_f^2 R_1 \omega^2 + M_f^2 \omega^2 R_f + R_1 R_2^2}{L_f^2 \omega^2 + R_2^2} \\ L_{It} = \frac{L_1 L_f^2 \omega^2 - M_f^2 \omega^2 L_f + L_1 R_2^2}{L_f^2 \omega^2 + R_f^2} \end{cases} \quad (9)$$

Based on (9), the equivalent resistance R_f and inductance L_f of the FO can be solved as

$$\begin{cases} L_f = \frac{M_f^2 \omega^2 (L_1 - L_{It})}{\omega^2 (L_1 - L_{It})^2 + (R_1 - R_{It})^2} \\ R_f = -\frac{M_f^2 \omega^2 (R_1 - R_{It})}{\omega^2 (L_1 - L_{It})^2 + (R_1 - R_{It})^2} \end{cases} \quad (10)$$

From (10), it can be concluded that L_f and R_f are determined by the mutual inductance M_f , since L_1 , R_1 , L_{It} and R_{It} can be measured. According to (3), M_f is related to the $R_{m,f}$ and $N_{m,f}$ which are both nonlinear. $R_{m,f}$ can be obtained from a FEM model. $N_{m,f}$ is decided by the distribution of eddy current which can also be simulated, while $N_{m,f}$ is not defined. Different definition of $N_{m,f}$ leads to different solutions of L_f and R_f . Whereas, it should be noticed that the definition of $N_{m,f}$ does not affect the value of the input impedance, which means the influence of different solutions on the DIPT system is the same.

According to (10), variables free from M_f can be obtained as

$$\begin{cases} \frac{R_f}{L_f} = -\frac{R_1 - R_{It}}{L_1 - L_{It}} \\ k = \frac{\sqrt{(L_1 - L_{It})L_1(\omega^2(L_1 - L_{It})^2 + (R_1 - R_{It})^2)}}{\omega L_1(L_1 - L_{It})} \end{cases} \quad (11)$$

It can be concluded from (11) that the ratio between R_f and L_f , and the coupling coefficient are independent of the value of M_f . Thus, these two variables can be directly measured from the terminal variables. Besides, since L_f and R_f are positive, L_{It} is smaller than L_1 , while R_{It} is larger than R_1 . The FO causes an increment of the input current leading phase and extra power losses to transfer the same amount of power.

TABLE I. IPT PROTOTYPE SPECIFICATIONS

Part	Property
Magnetic Core	Material: Ferrite N87 Number of bars: 3
Litz wire	Type: AWG 41 Number of strands: 525
Coil	Number of turns: 30

IV. EXPERIMENTAL ANALYSIS

A. Measurements

The measurement is carried out on a 3.3 kW IPT prototype using DD topology on both sides. The impedance analyzer (Agilent 4294A, 40 Hz to 110 MHz) is used. The compensation capacitors are not connected. The design specification is presented in Table I. By using the impedance analyzer, the terminal inductances ($L_{1t, mis}$, $L_{2t, mis}$) and mutual inductance (M_{mis}) are obtained. As shown in Fig. 6, seven misalignment points are selected along the x-axis and y-axis. Under each test point, the terminal inductances of both primary and secondary pads are measured as shown in Fig. 7(a). The mutual inductance is derived from the total terminal inductance when the primary and secondary pads are connected as in Fig. 7(b). Regarding the measurements with FO, a thin planar copper object (9.4 cm*4.6 cm) is selected and the charging pads are perfectly aligned. The terminal inductances ($L_{1t, f}$, $L_{2t, f}$) and mutual inductance (M_f) are derived as Fig. 7(c) and 7(d). Three FO conditions are considered, i.e., no FO inserted, centered FO and sided FO. Because the distribution of the eddy current within the FO is dependent on the field frequency. A frequency sweeping is carried out in the measurements to consider the fundamental order 85 kHz, third order 255 kHz, fifth order 425 kHz and seventh order 595 kHz. The results are shown in Fig. 8, 9 and 10.

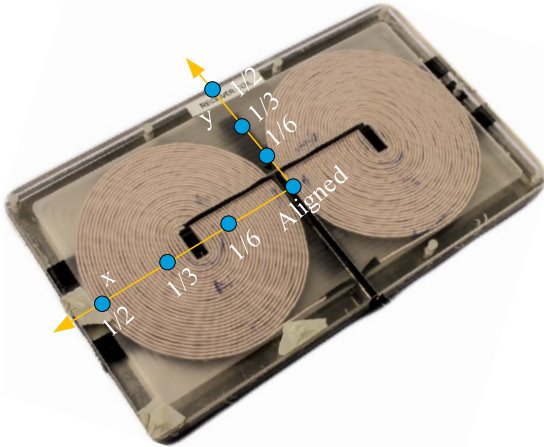


Fig. 6. 3.3 kW charging pad and misalignment points.

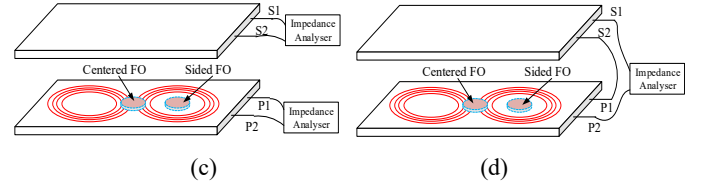
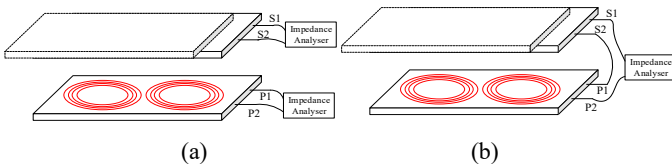


Fig. 7. Impedance measurements. (a) pad terminal inductance under misalignment, (b) mutual inductance under misalignment, (c) pad terminal inductance with FO, (d) mutual inductance with FO.

B. Analysis

In Fig. 8, the terminal inductance shows a clear positive correlation with the frequency. The terminal inductance contains the contribution from the parasitic capacitance, aluminium shield and ferrite. As the frequency increases, the negative contribution of parasitic capacitance reduces, while the influence of eddy current is not comparable at the discussed frequency range. Therefore, the terminal pad inductance increases over frequency. In Fig. 8(c), the primary terminal inductance of sided FO shows a constant negative offset, compared with the other two curves. This occurs because the flux at the sided point is almost perpendicular to the surface of the FO, which implies a strong mutual coupling. This can be verified in (9) where M_f hold a negative relation to L_{1t} .

In Fig. 9(a), the mutual inductance of the misalignment case shows a positive correlation with the frequency, while an opposite trend is presented under the FO condition. As the frequency increase, the eddy current of aluminum shielding plays an important role in the discussed frequency range. Because the shielding is placed outside the air gap, the eddy current with the shielding forces the magnetic field to the air gap, which can be explained by (6). However, the FO is placed inside the air gap, so the mutual inductance decreases as the frequency becomes higher, as shown in Fig. 9(b). It should be noticed that the coupling between FO and the primary charging pad increases as the frequency rises, which is in accordance to (3).

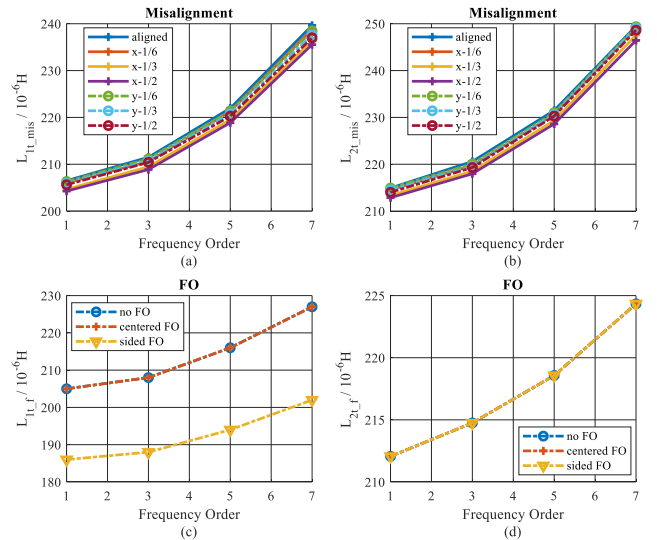


Fig. 8. Charging pad terminal inductance. (a) primary pad and (b) secondary pad under misalignment, (c) primary pad and (d) secondary pad with FO.

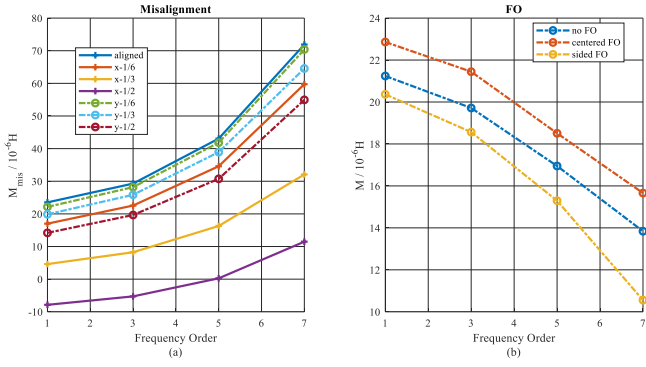


Fig. 9. Mutual inductance between charging pads. (a) misalignment, (b) FO.

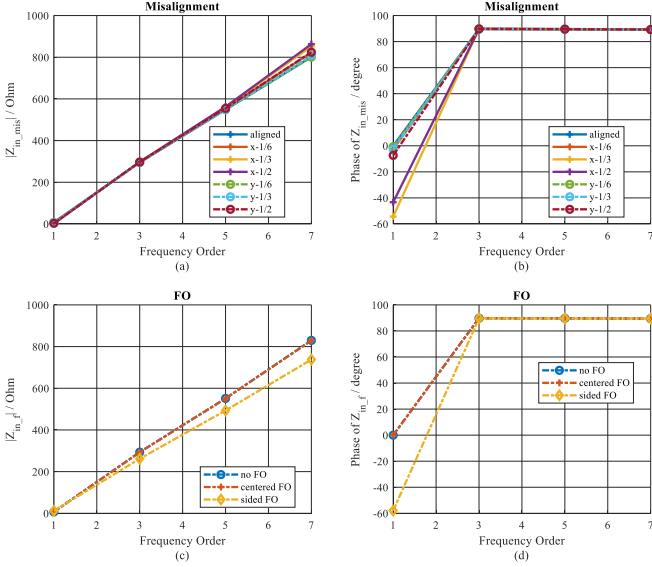


Fig. 10. Primary input impedance. (a) absolute value and (b) phase under misalignment, (c) absolute value and (d) phase with FO.

The input impedance is calculated based on the measurements. C_1 and C_2 which are tuned at 85 kHz without misalignment and FO, as well as 20 Ohm R_{load} are included in the input impedance. The input impedance under both misalignment and FO conditions which are shown in Fig. 10 have a similar behavior. Under the worst condition, the impedance becomes capacitive under fundamental frequency due to the reduction of terminal inductance caused by misalignment and FO. At high order frequency, the AC resistance and the capacitive part of the input impedance are not comparable to the inductive part, so the input impedance appears to be purely inductive. Regarding the absolute value of the input impedance, it is noticeable that the curve of the largest misalignment is above others, while the curve of the sided FO is below others. For the misalignment case, the inductive part of the input impedance can be derived from (8). At high frequency range, the capacitance from the compensated capacitor is negligible, so the inductive part of the input impedance can be expressed as

$$\text{Im}(Z_{in_mis}) \approx \omega L_1 - \frac{\omega^3 M^2 L_2}{R_{load}^2 + \omega^2 L_2^2} \quad (12)$$

As the misalignment increases, the mutual inductance decreases significantly and its square value plays as dominant role in (12). Besides, at high frequency point, the resistive part of the input impedance is not comparable to the inductive part. Thus, the largest impedance happens at the worst misalignment condition. For the FO case, the sided FO causes a reduction of the primary terminal inductance as shown in Fig. 8(c). Therefore, the smallest impedance happens when the FO is placed at the sided point.

C. Discussions

It can be concluded that both misalignment and FO can change the primary input impedance, but the contribution of misalignment to the absolute value of the impedance is positive while that of FO is negative. Besides, the terminal inductance of the primary pad shows a noticeable decrement when FO is placed at the sided point. By contrast, the influence of misalignment is negligible. Regarding the relation between mutual inductance and frequency, the influence of FO and misalignment shows an opposite trend.

Based on the difference illustrated above, it is possible to detect the FO through the variation of the primary terminal inductance, as well as the frequency dependence of the input impedance and the mutual inductance.

V. HARMONICS ANALYSIS

A. Analysis of the current harmonics

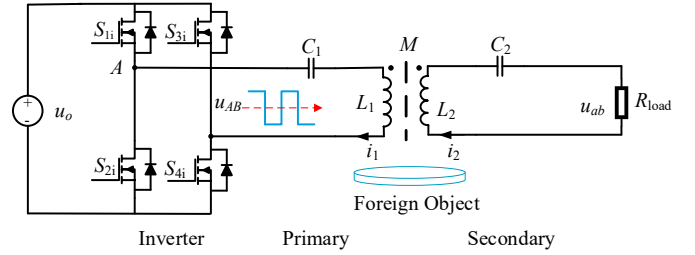


Fig. 11. IPT system schematic.

Apart from detecting the variation of the system parameters discussed in Section IV, the waveform distortion of the inverter output current also provides a possibility to detect FO. According to the parameters measured from the prototype, the THD of the input current can be calculated. The equivalent circuit is shown in Fig. 11. It is assumed that the inverter output voltage is a square waveform and capacitor C_1 and C_2 are tuned for the resonance under fundamental frequency. The Fourier series of the inverter output voltage u_{AB} is

$$u_{AB} = U_{AB} \sum_{k=0,1,\dots} \frac{\sin((2k+1)\omega_0 t)}{2k+1} \quad (13)$$

where U_{AB} is the amplitude of u_{AB} . Using the input impedance in (5), the current harmonics can be obtained as

$$\begin{cases} I_{1_{(2k+1)th_f}} = \frac{4U_{AB} \sin(n\omega_0 t)}{n\pi(j\omega_0 L_1(n - \frac{1}{n}) + \frac{n^2 \omega_0^2 k^2 L_1 L_2}{j\omega_0 L_2(n - \frac{1}{n}) + R_{load}} + \frac{n^2 \omega_0^2 k_f^2 L_1 L_f}{jn\omega_0 L_f + R_f})} \\ I_{1_{(2k+1)th_mis}} = \frac{4U_{AB} \sin(n\omega_0 t)}{n\pi(j\omega_0 L_1(n - \frac{1}{n}) + \frac{n^2 \omega_0^2 k^2 L_1 L_2}{j\omega_0 L_2(n - \frac{1}{n}) + R_{load}})} \end{cases} \quad (14)$$

In this paper, only the third, fifth and seventh harmonics are considered. The THD of the inverter output current is

$$THD = \frac{\sqrt{I_{1_3rd}^2 + I_{1_5th}^2 + I_{1_7th}^2}}{I_{1_1st}} \quad (15)$$

The THD is shown in Fig. 12. It can be seen that THD is less as the misalignment become larger except for the point x-1/2. This can be explained by Fig. 10(a) where the absolute value of the input impedance is larger as the misalignment becomes larger at the same frequency. Accordingly, as shown in (14), the amplitude of the current harmonics becomes smaller. For the points x-1/3 and x-1/2, the coupling between the charging pads is almost zero, so there is no clear differences. Thus, the THD of both two points lies close to the lower boundary.

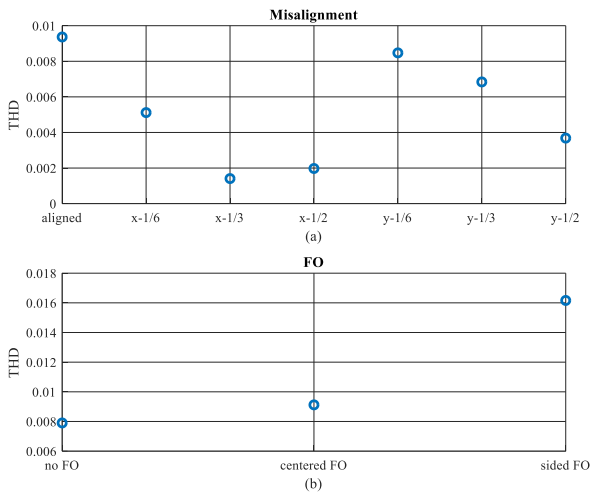


Fig. 12. THD of the input current. (a) misalignment, (b) FO.

On the contrary, the waveform distortion increases with the presence of the FO. It can be explained by Fig. 10(c) where the absolute value of the input impedance decrease when FO is presented. In fact, the impedance of high frequency is decided by the terminal inductance of the primary coil which is reduced by the coupling between FO and the primary pad, as indicated by (9). Thus, the presence of the FO increases the content of current harmonics. Besides, the coupling at sided point is stronger than that of the centered point. Therefore, the THD at sided point is larger.

B. Discussions

As shown in Fig. 12, the THD of the inverter output current keeps below 1% under all conditions. In Fig. 11, the rectifier is not included. The rectifier normally introduces more current

harmonics. Therefore, the variation of THD caused by FO and misalignment is difficult to be distinguished.

VI. CONCLUSION

This paper studies the effect of the copper FO and the misalignment on the IPT system parameters and current harmonics. Through the analysis the influence of FO and misalignment on the mutual inductance, input and terminal impedances and current harmonics are explained. Finally, through the measurements of a 3.3 kW IPT prototype the proposed analysis is verified. Based on the results, it can be concluded that: 1) FO causes a clear reduction of the primary pad terminal inductance while misalignment results in only slightly difference. 2) the mutual inductance under FO condition has a negative correlation to the frequency, while that of misalignment is positive. 3) when compensation is considered, FO leads to a reduction of the primary input impedance, while misalignment increases the primary input impedance. 4) the influence of both FO and misalignment on current harmonics is minimal. According to the features above, it is possible to detect FOs and distinguish it from a misalignment condition, through the variation of the primary terminal inductance, as well as the frequency dependence of the input impedance and the mutual inductance.

ACKNOWLEDGMENT

The results presented in this paper are developed in the framework of the 16ENG08 MICEV Project. The latter received funding from the EMPIR programme co-financed by the Participating States and from the European Union's Horizon 2020 research and innovation programme.

REFERENCES

- [1] J. Deng, B. Pang, W. Shi, and Z. Wang, "A new integration method with minimized extra coupling effects using inductor and capacitor series-parallel compensation for wireless EV charger," *Applied Energy*, vol. 207, pp. 405–416, Dec. 2017.
- [2] S. Fukuda, H. Nakano, Y. Murayama, T. Murakami, O. Kozakai, and K. Fujimaki, "A novel metal detector using the quality factor of the secondary coil for wireless power transfer systems," in *2012 IEEE MTT-S International Microwave Workshop Series on Innovative Wireless Power Transmission: Technologies, Systems, and Applications*, 2012, pp. 241–244.
- [3] H. Kikuchi, "Metal-loop effects in wireless power transfer systems analyzed by simulation and theory," in *2013 IEEE Electrical Design of Advanced Packaging Systems Symposium (EDAPS)*, 2013, pp. 201–204.
- [4] N. Kuyvenhoven, C. Dean, J. Melton, J. Schwannecke, and A. E. Umenei, "Development of a foreign object detection and analysis method for wireless power systems," in *2011 IEEE Symposium on Product Compliance Engineering Proceedings*, 2011, pp. 1–6.
- [5] S. Y. Jeong, H. G. Kwak, G. C. Jang, S. Y. Choi, and C. T. Rim, "Dual-Purpose Nonoverlapping Coil Sets as Metal Object and Vehicle Position Detections for Wireless Stationary EV Chargers," *IEEE Transactions on Power Electronics*, vol. 33, no. 9, pp. 7387–7397, Sep. 2018.
- [6] S. Verghese, M. P. Kesler, K. L. Hall, and H. T. Lou, "Foreign object detection in wireless energy transfer systems," *US9442172B2*, 13-Sep-2016.
- [7] C. T. Rim and C. Mi, "Foreign Object Detection," in *Wireless Power Transfer for Electric Vehicles and Mobile Devices*, IEEE, 2017.